Bonding of Cast Iron-Aluminum In Bimetallic Castings By High Pressure Die Casting Process

Mengwu Wu (wumw@whut.edu.cn)
Wuhan University of Technology
Jinpeng Yang
Wuhan University of Technology
Feng Huang
Wuhan University of Technology
Lin Hua
Wuhan University of Technology
Shoumei Xiong
Tsinghua University

Research Article

Keywords: High pressure die casting, Bimetallic casting, Bonding interface, Aluminum, Cast iron

Posted Date: October 26th, 2021

DOI: https://doi.org/10.21203/rs.3.rs-1002236/v1

Version of Record: A version of this preprint was published at The International Journal of Advanced Manufacturing Technology on February 2nd, 2022. See the published version at https://doi.org/10.1007/s00170-022-08816-x.

Abstract

A practical bimetallic casting consisting of aluminum matrix and cast iron inserts was manufactured via high pressure die casting (HPDC) process. Different surface treatment methods of the cast iron inserts, including salt membrane plating and electrogalvanizing, were adopted to improve the bonding quality of bimetallic castings. Microstructure characterization on the bonding interface was conducted at different locations of bimetallic castings. Results indicate that compounds with flawless and continuously metallurgical bonding interface can be successfully fabricated by the HPDC process with the zinc rack plating treatment on the surface of cast iron inserts which results in a dense zinc coating with an average thickness of 8 μm. The melt flow speed and heat transition during solidification of the HPDC process are two key factors in determining the bonding integrity of bimetallic castings. With the dissolution and diffusion of the very thin zinc coating during solidification, there is no obvious aggregation of zinc element at the metallurgical bonding interface. Instead, a reaction layer with an irregular tongue-like morphology is formed with an average thickness of approximately 1 μm while it mainly consists of intermetallic phases $Al_{60}Cu_{30}Fe_{10}$ and Al_2FeSi, etc.

1 Introduction

Bimetallic materials generally have superior comprehensive properties which are extremely difficult to achieve for single metal materials [1–3]. Comparing to other bimetal bonding processes, the solid-liquid bimetal compound casting has been extensively used in modern industry with the advantages of good interfacial bonding quality, high production efficiency and wide range of applicable alloys, etc. [4–7]. For instance, the most typical application of this process in automotive is the manufacturing of aluminum engine cylinder block with cast iron liners. Fe-Al bimetallic cylinder block has been a subject of investigation for more than twenty years due to its excellent performance on lightweight and thermal conductivity comparing to the traditional cast iron cylinder block [8, 9].

The challenge of solid-liquid compound casting is the realization of a firmly bonding between two metal components. The characteristic of a real “compound cast” part is the formation of metallurgical bonding interfacial zones where the cast alloy’s components diffuse into the solid material partly via the formation of solid solutions, and partly via the formation of reaction phases [10–14]. It has been proposed that an excellent metallurgical interface is of great importance to guarantee the physical and mechanical properties of bimetallic castings [15–18]. However, due to the difference in the thermal-physical properties, metallurgical bonding is extremely difficult to achieve for compound casting of dissimilar metals. Even for similar metallic couples, owing to the formation of oxide layer on surface of the solid substrate, the wettability between solid-state and liquid-state metals is largely impaired, leading to an incompatible and poor bonding between two metal components [19, 20]. There are a number of attempts to protect the surface of solid substrate metals from oxidation and to obtain an excellent metallurgical bonding between similar and also dissimilar metallic couples. Jiang et al. [21] found that a surface treatment method of steel inserts, i.e., a combination of coating surface modifier and aluminizing, could promote the formation of a metallurgical bonding interface between carbon steel and ZL114A

aluminum alloy during compound casting process. Koerner et al. [22–24] pointed out that wrought Al-cast Al bimetallic castings with flawless metallic interface can be successfully produced by replacing the oxide layer on surface of wrought Al substrate with a zinc layer. Feng et al. [25] investigated the influence of coating materials on the overcast joining of aluminum alloys and concluded that Ni coating was superior over Cu coating. Ren et al. [26, 27] reported that Al-Mg bimetallic castings could be successfully fabricated by solid-liquid compound casting and they studied the effect of pouring temperature on the interficial microstructure and mechanical properties of overcast joints.

According to literature review, most of the existing research works relating to the solid-liquid compound casting are based on the sand mould or permanent mould casting process. The HPDC process is the preferred choice for the mass production of light metal castings in the automotive, electronics, communications and other fields [28–31]. Comparing to the sand mould and permanent mould casting processes, the much shorter heating and cooling times during the HPDC process represent a great challenge for the solid-liquid bimetal compound casting. Since the time is extremly inadequate for the diffusion and reaction between the two metal alloys during solidification of the HPDC process, it is difficult to achieve metallurgical bonding for bimetallic castings. Accordingly, the fabrication of bimetallic castings by using the HPDC process is still a relatively unexplored area, especially for the Fe-Al bimetallic castings while there are large differences between the two types of metals relating to the thermal-physical properties, including the melting point.

In this study, a practical bimetallic casting consisting of aluminum matrix and cast iron inserts was manufactured by the HPDC process. Different surface treatment methods of the cast iron inserts were adopted to improve the bonding quality of bimetallic castings. Microstructure characterization on the bonding interface of bimetallic castings and simulation of the HPDC process were both conducted, based on which the effects of surface treatment methods and casting process on the bonding quality of bimetallic castings were investigated.

2 Experimental

2.1 Materials and surface treatment

A practical bimetallic casting named “bottom cylinder block” with complex structure was produced as shown in Fig. 1. For lightweight purpose, the component is mostly made of A380 aluminum alloy, while the part of bearing housing is made of HT250 gray cast iron to reduce friction between the crankshaft and bearing housing and to increase local strength. According to the analysis of Inductive Coupled Plasma (ICP) and C-S analyzer, the chemical compositions of A380 aluminum alloy and HT250 gray cast iron are listed in Table 1 and Table 2, respectively.

In order to improve the bonding quality of bimetallic castings, different surface treatment methods were used for the gray iron inserts. The main purpose of surface treatment is to protect the solid metal surface from oxidation and to enhance the wettability of aluminum melt on its surface. The surface treatment

methods used in this study include salt membrane plating and electrogalvanizing. Firstly, the surface of the gray iron inserts was sandblasted to remove oxides, and then rinsed using a 0.5 mol/L hydrochloric acid and an ethanol, respectively. After being cleaned, the gray iron inserts were immersed into a solution of sodium chloride and ammonium chloride with a weight ration of 1:1 and a total concentration of 100 g/L at 50 ° C for 15 minutes. Afterwards, the gray iron inserts were taken out and dried. Another surface treatment method after the gray iron inserts being cleaned was electrogalvanizing with an electrolyte containing 150 g/L $ZnSO_4$, 50 g/L $N_2H_8SO_4$ and 15 g/L boric acid. Different thicknesses of zinc coating were expected to obtained by the barrel plating and rack plating processes. With the same current density of 30 mA/cm^2 at room temperature, the time for barrel plating was 1 hour, 2 hours and 3 hours, respectively, while the time for rack plating was 1 hour. Consequently, six groups of experiments were constructed in this study according to different surface treatment methods of gray iron inserts as shown in Table 3.

Table 1
Chemical composition of the A380 aluminum alloy (wt%)

Si	Cu	Fe	Mn	Mg	Zn	Ni	Sn	Al
9.01	3.25	1.25	0.19	0.14	0.99	0.06	0.02	Bal.

Table 2
Chemical composition of the HT250 gray cast iron (wt%)

C	Si	Mn	S	P	Fe
3.08	1.92	0.99	0.08	0.03	Bal.

Table 3
Six groups of experiments distinguished by the surface treatment methods of gray iron inserts

Code	Surface treatment
1#	No treatment except for being cleaned
2#	Salt membrane plating
3#	Zinc barrel plating for 1 hour
4#	Zinc barrel plating for 2 hours
5#	Zinc barrel plating for 3 hours
6#	Zinc rack plating for 1 hour

2.2 Casting process

Once the surface treatment process was completed, the gray iron inserts were heated to 200 ℃ by means of electromagnetic induction and then rapidly placed inside the die casting mold for pouring. A UB1650iV

cold chamber die casting unit was used for the fabrication of bimetallic castings. In order to balance the requirements of a sound metallic bonding and a good overall quality of the bimetallic castings, key process parameters used during the HPDC process were set as: pouring temperature of the aluminum melt (650 ℃), initial mold temperature (200 ℃) and intensification casting pressure (80 MPa). With a diameter of 130 mm, the plunger was first moving in a speed constantly accelerated from 0 to 0.3 m/s for 522 mm at the slow shot stage. Then the plunger speed was rapidly accelerated to 3.4 m/s and the HPDC process stepped into the fast shot stage. Intensification casting pressure was applied when the plunger was moving to 750 mm and maintained until the casting solidified.

2.3 Microstructure characterization

To investigate the bonding quality and interfacial microstructure of the bimetallic castings, metallographic specimens were cut from the bimetallic castings as illustrated in Fig. 1. Since there were five gray iron inserts in the bimetallic castings, the rightmost one was chosen to analyze the bonding quality with the aluminum matrix. Due to the complex structure of both the gray iron insert and aluminum matrix, seven bonding interfaces marked “A1”, “A2”, “A3”, “A4” and “B1”, “B2”, “B3” from two sections were selected for comparative study. A ZEISS scope A1 optical microscope (OM), a JSM-IT300 scanning electron microscope (SEM) equipped with energy disperse spectroscopy (EDS) and a FEI Talos F200X transmission electron microscope (TEM) were used for metallography observation. The metallographic specimens were treated following the standard metallographic procedures and etch was not required.

3 Results

3.1 Surface morphology of the gray iron inserts

Figure 2 shows the surface macro-morphology of gray iron inserts with different surface treatment methods. By sandblasting and cleaning, the surface of the gray iron insert in Fig. 2(a) reveals its natural color. An obvious salt membrane is formed on the surface of the gray iron insert as shown in Fig. 2(b). It has been reported that the use of a sodium chloride solution or ammonium chloride solution is favorable to the removal of oxide layer generated at the surface of gray iron inserts by chemical reaction [21]. Meanwhile, the salt membrane acts as a barrier to prevent the gray iron inserts from further oxidation, thereby enhancing the wettability between the gray iron inserts and aluminum melt. By the surface treatment method of electrogalvanizing, either through barrel plating or rack plating process, the surface of the gray iron insert in Fig. 2(c) exhibits a metallic luster of zinc. It has been proved that zinc is well suited as a coating material for the solid-liquid bimetal compound casting [23]. The oxidation of zinc will result in the formation of a thin but dense zinc oxide film, which can effectively prevent the inner zinc metal and gray iron inserts from oxidation. Other significant advantages of zinc include a relative low melting temperature of 420 ℃ and a high solubility in aluminum at elevated temperature. These crucial properties are beneficial to the diffusion and chemical reaction between the gray iron inserts and molten aluminum alloy.

It is known that the quality of zinc coating formed by electrogalvanizing is deeply related to the specific electroplating process and the corresponding process parameters. Figure 3 shows the cross section morphology of zinc coating on surface of gray iron inserts with different electrogalvanizing processes. It can be seen from Fig. 3(a-c) that with the increase of the time for barrel plating from 1 hour to 2 and 3 hours, the average thickness of the zinc coating increases from 1 μm to 2.5 μm and 4.5 μm. For rack plating with 1 hour, the average thickness of the zinc coating increases to 8 μm as shown in Fig. 3(d). Figure 4 indicates the surface micro-morphology of the gray iron inserts with different electrogalvanizing processes. In combination with the corresponding EDS mapping results, it can be concluded that for zinc coating, the variation trend of coating density is consistent with the thickness mentioned above. With barrel plating for 1 hour, the surface of the zinc coating is very uneven as noted in Fig. 4(a). A sparse zinc coating leads to a large number of iron atoms to be exposed to the surface (Fig. 4(b-c)). This situation is substantially improved by increasing the time for barrel plating from 1 hour to 2 and 3 hours. For rack plating with 1 hour, a dense zinc coating is obtained as shown in Fig. 4(j-l), which is considered beneficial for protecting the gray iron inserts from oxidation and enhancing the wettability between the gray iron inserts and aluminum melt.

3.2 Bonding quality of the bimetallic castings

Microstructure characterization on the bonding interfaces was conducted to investigate the effect of surface treatment methods of the cast iron inserts on the bonding quality of bimetallic castings. Corresponding to the six experimental groups listed in Table 3, Figure 5 shows the interfacial microstructure at the bonding interface “A4” of bimetallic castings with different surface treatment methods of the gray iron inserts. A large gap with a width more than 20 μm is observed in the interfacial microstructure of bimetallic casting with no treatment except for being cleaned of the gray iron inserts as shown in Fig. 5(a), leading to an incompatible and poor bonding between two metal components. By salt membrane plating of the gray iron inserts, the gap between the two metal components becomes narrow as illustrated in Fig. 5(b). However, a large number of inclusions, perhaps salt membrane residues, are observed in the interfacial microstructure, resulting in a poor integrity of the bimetallic castings. With zinc barrel plating of the gray iron inserts, the bonding quality of bimetallic castings is improved. Particularly, the gap width between the two metal components continues to decrease with the increase of the time for zinc barrel plating from 1 hour to 2 and 3 hours as noted in Fig. 5(c-e). In the case of zinc rack plating for 1 hour, the integrity of the compound interface of bimetallic castings is greatly increased. With the disappearance of the gap, a reaction layer forms between the two metal components as shown in Fig. 5(f), which indicates that compounds with flawless and continuously metallurgical bonding interface are successfully fabricated.

To reveal the detailed characteristics of the reaction layer between the two metal components in Fig. 5(f), high-magnification interfacial microstructure is observed by SEM as shown in Fig. 6. The reaction layer exhibits an irregular tongue-like morphology with an average thickness of approximately 1 μm. According to the EDS line scanning results, the distribution of the elements Al and Fe conforms to the Fick’s law of diffusion [32], i.e., the contents of Al and Fe decrease gradually along the thickness of the reaction layer,

respectively in the directions from the aluminum matrix to the gray iron insert and the opposite one. This phenomenon proves that diffusion and reaction between the two metal alloys undoubtedly happen during solidification of the compound casting process, which are essential and important conditions to guarantee a metallurgical bonding of the bimetallic castings.

Since the bimetallic castings in this study are practical products with complex structures of both the gray iron insert and aluminum matrix, the bonding quality may vary greatly at different joint locations. Figure 7 illustrates the microstructure at different bonding interfaces of the bimetallic casting with a treatment of zinc rack plating for 1 hour on surface of the gray iron inserts. It can be seen from Fig. 7(a-d) that among the four bonding interfaces in section A, only the bonding interface “A4” conforms to the characteristics of metallurgical bonding, while large gaps appear in the microstructure at the bonding interfaces “A1” and “A3”. For section B as shown in Fig. 7(e-g), the reaction layer is observed both at the bonding interfaces “B2” and “B3”. In particular, the bonding interface “B2” is flawless with continuously metallurgical bonding, which is the ideal state to expect for bimetallic castings with superior comprehensive properties. As for the reason for the difference of the bonding quality between these bonding interfaces, this will be discussed in detail in the following section.

3.3 Phase distribution in the interfacial layer

To investigate the diffusion and reaction behavior between the two metal alloys during solidification of the compound casting process, element and phase distribution in the interfacial layer with metallurgical bonding was extracted by TEM and EDS as shown in Fig. 8 and Table 4. The TEM bright-field image (Fig. 8(a)) is clearly divided into three parts by the reaction layer with an irregular tongue-like morphology. They are the A380 aluminum alloy matrix, the reaction layer and HT250 gray iron insert from top to bottom. It can be seen from Fig. 8(c-f) and Table 4 that except for elements Al and Fe, there also exists the diffusion and reaction of Cu and Si in the reaction layer. Here, the reaction layer is just the so-called intermetallic compound (IMC) layer where the elements mentioned above exist in the form of intermetallic compound. Most of the elements Al and Si come from the A380 aluminum alloy matrix by diffusion. Different from the element Si in the microstructure of A380 aluminum alloy in the form of primary or eutectic Si phase, it is in the form of intermetallic compound, resulting in a uniform distribution in the reaction layer on a micron level. Due to a high melting point of the HT250 gray iron, the diffusion of the element Fe is extremely difficult which leads to a relative low content in the reaction layer. It is noteworthy that the element Cu unexpectedly accumulates in the reaction layer. According to the EDS analysis in Table 4, the content of Cu in the reaction layer is even higher than that of the A380 aluminum alloy matrix where it comes from by diffusion. This may be because the radius of the Cu atom is much closer to that of the Fe atom comparing to the radius of the Al atom, which facilitates the diffusion of Cu atoms from A380 aluminum alloy matrix towards the reaction layer. Another phenomenon is also retrieved from Fig. 8 and Table 4 that there is no obvious aggregation of the element Zn in the interfacial layer with metallurgical bonding.

Figure 8(b) shows the electron diffraction pattern of point 3 marked in Figure 8(a). In combination with the EDS analysis in Table 4, the phase at point 3 is identified to be $Al_{60}Cu_{30}Fe_{10}$. In fact, the phase

distribution in the interfacial layer is extremely complex due to the reaction of the multiple elements with each other which leads to the formation of multiple intermetallic compounds. Other phases in the reaction layer may include Fe_2Al_5, $FeAl_3$ and Al_2FeSi, etc. [9, 21]. The formation of intermetallic phases is related to the mixing enthalpy between different elements, while the lower the mixing enthalpy, the more likely the corresponding intermetallic phase will form accompanied with the release of latent heat.

Table 4 EDS analysis results corresponding to the points indicated in Fig. 8(a)

Number	Element compositions（at%）						
	Al	Fe	Cu	Si	C	Mn	Zn
Point 1	79.8	0.09	16.97	1.74	0.23	0.04	0.98
Point 2	53.15	12.88	21.51	9.18	1.62	1.22	0.34
Point 3	58.06	10.66	21.07	7.3	1.48	0.65	0.44
Point 4	20.98	48.31	18.89	6.4	3.64	0.42	1.25
Point 5	1.14	74.1	16.11	3.61	4.17	0.67	0.04

4 Discussion

It is well known that the metallurgical bonding of bimetallic castings is guaranteed by the formation of a diffusion reaction zone between the two metallic materials. Due to the large difference of the thermal-physical properties between Fe and Al, as well as the oxide film formed at the surface of solid inserts, it is difficult to achieve metallurgical bonding for Fe-Al bimetallic castings. Furthermore, the challenge is significantly increased with the adoption of the HPDC process in the solid-liquid bimetal compound casting. In this aspect, the present work is meaningful while cast iron-aluminum compounds with flawless and continuously metallurgical bonding interface is successfully fabricated by the HPDC process with a zinc rack plating treatment on the surface of cast iron inserts. However, for the practical bimetallic casting in this study with complex structures of both the gray iron insert and aluminum matrix, not all bonding interfaces achieve metallurgical bonding as indicated in Fig. 7. The cause of this phenomenon may be ascribed to the difference in solidification conditions at these interfaces. Except for a sufficient thick and dense zinc coating to protect the gray iron inserts from oxidation, appropriate thermodynamic conditions of the aluminum melt are also required for the metallurgical bonding between the two metallic materials. Accordingly, the Anycasting software was used to analyze the filling and solidification process of the aluminum melt during the HPDC process in present work.

Figure 9 shows the simulated results of mold filling near section A at different times. It can be seen that the interfaces “A1” and “A3” are perpendicular to the melt flow direction. Due to the influence of the cavity structure, the melt flow direction dramatically changes near the interface “A2”, resulting in air entrapment

in the aluminum melt as shown in Fig. 9(c-d). Comparatively, the melt flow near the interface “A4” is the most ideal with a flow direction parallel to the interface. Figure 10 shows the simulated quantitative results of the melt flow speed and temperature at different interfaces. It can be noted from Fig. 10(a) that the melt flow speed at interface “A4” is much higher than that at the other three interfaces. Since only the interface “A4” conforms to the characteristics of metallurgical bonding as shown in Fig. 7(a-d), it can be concluded that a high melt flow speed is beneficial to the formation of metallurgical bonding interface between the two metallic materials. Combining the metallographic results as indicated in Fig. 7(e-g) and the simulated results as shown in Fig. 10(b), a similar conclusion also can be made that the flawless and continuously metallurgical bonding of interface “B2” is due to a much lower cooling rate and slower drop of the temperature of the aluminum melt comparing to those at the other two interfaces.

According to the analysis mentioned above, the melt flow speed and heat transition during solidification of the HPDC process are two key factors in determining the bonding integrity of bimetallic castings. With a high flow speed and temperature of the aluminum melt, a large amount of thermal shock acts upon the gray iron inserts, resulting in the dissolution and diffusion of the zinc coating. This can be additionally elucidated in Fig. 11. No obvious aggregation of the element Zn is detected in the interfacial layer with metallurgical bonding, but a considerable amount of it remains at the interface without metallurgical bonding. With the sufficient dissolution and diffusion of the zinc coating, the fresh and clean surface of gray iron inserts is exposed, which is beneficial to the diffusion and reaction between the two metallic materials. Meanwhile, studies have shown that a too thick zinc coating is not conducive to a firmly metallurgical bonding of bimetallic castings [23].

5 Conclusions

In this study, the effects of surface treatment methods of the gray iron inserts and casting process on the bonding quality of a practical bimetallic casting have been investigated. The following conclusions can be drawn:

(1) With the rack plating process for 1 hour, a dense zinc coating is formed on surface of the gray iron inserts with an average thickness of 8 μm.

(2) Cast iron-aluminum compounds with flawless and continuously metallurgical bonding interface can be successfully fabricated by the HPDC process with the zinc rack plating treatment on the surface of cast iron inserts.

(3) The melt flow speed and heat transition during solidification of the HPDC process are two key factors in determining the bonding integrity of bimetallic castings. With the dissolution and diffusion of the very thin zinc coating during solidification, there is no obvious aggregation of zinc element at the metallurgical bonding interface, while the content of Cu is higher than that of the A380 aluminum alloy matrix where it comes from by diffusion.

(4) In the interfacial microstructure of bimetallic castings with metallurgical bonding, a reaction layer with an irregular tongue-like morphology is formed with an average thickness of approximately 1 μm consisting of intermetallic phases $Al_{60}Cu_{30}Fe_{10}$ and Al_2FeSi, etc.

Declarations

Acknowledgments

This work was financially supported by the National Natural Science Foundation of China (No. 51805389), Higher Education Discipline Innovation Project (B17034) and Hubei Key Laboratory of Advanced Technology for Automotive Components, Wuhan University of Technology (XDQCKF2021011).

References

1. Jiang SY, Zhang YQ, Zhao YA et al (2017) Investigation of interface compatibility during ball spinning of composite tube of copper and aluminum. Int J Adv Manuf Technol 88(1-4):683–690
2. Shen YY, Jia Q, Zhang X et al (2021) Tensile behavior of SiC fiber-reinforced gamma-TiAl composites prepared by suction casting. Acta Metall Sin (Engl Lett) 34(7):932–942
3. Jin K, Yuan QW, Tao J et al (2019) Analysis of the forming characteristics for Cu/Al bimetal tubes produced by the spinning process. Int J Adv Manuf Technol 101(1-4):147–155
4. Hu Q, Jiang ZL, Jiang WM et al (2019) Interface characteristics of Mg/Al bimetal produced by a novel liquid-liquid compound casting process with an Al interlayer. Int J Adv Manuf Technol 101(5-8):1125–1132
5. Liu T, Wang QD, Sui YD et al (2016) An investigation into interface formation and mechanical properties of aluminum-copper bimetal by squeeze casting. Mater Des 89:1137–1146
6. Liu GP, Wang QD, Liu T et al (2017) Effect of T6 heat treatment on microstructure and mechanical property of 6101/A356 bimetal fabricated by squeeze casting. Mater Sci Eng A 696:208–215
7. Ding ZY, Zhang NF, Yu L et al (2021) Recent progress in metallurgical bonding mechanisms at the liquid/solid interface of dissimilar metals investigated via in situ X–ray imaging technologies. Acta Metall Sin (Engl Lett) 34(2):145–168
8. Jiang WM, Fan ZT, Li GY et al (2016) Effects of hot-dip galvanizing and aluminizing on interfacial microstructures and mechanical properties of aluminum/iron bimetallic composites. J Alloy Compd 688:742–751
9. Springer H, Kostka A, Payton EJ et al (2011) On the formation and growth of intermetallic phases during interdiffusion between low-carbon steel and aluminum alloys. Acta Mater 59(4):1586–1600
10. Liu T, Wang QD, Sui YD et al (2016) Microstructure and mechanical properties of overcast 6101-6101 wrought Al alloy joint by squeeze casting. J Mater Sci Technol 32(4):298–304
11. Xu JZ, Gao XJ, Jiang ZY et al (2016) Microstructure and hot deformation behaviour of high-carbon steel/low-carbon steel bimetal prepared by centrifugal composite casting. Int J Adv Manuf Technol

86(1-4):817–827

12. Zhu ZA, Shi RH, Klarner AD et al (2020) Predicting and controlling interfacial microstructure of magnesium/aluminum bimetallic structures for improved interfacial bonding. J Magnes Alloy 8(3):578–586
13. He K, Zhao JH, Li P et al (2016) Investigation on microstructures and properties of arc-sprayed-Al/AZ91D bimetallic material by solid-liquid compound casting. Mater Des 112:553–564
14. Zhang H, Chen YQ, Luo AA (2014) A novel aluminum surface treatment for improved bonding in magnesium/aluminum bimetallic castings. Scr Mater 86:52–55
15. Zare GR, Divandari M, Arabi H (2013) Investigation on interface of Al/Cu couples in compound casting. Mater Sci Technol 29(2):190–196
16. Jiang WM, Fan ZT, Li GY et al (2016) Effects of zinc coating on interfacial microstructures and mechanical properties of aluminum/steel bimetallic composites. J Alloys Compd 678:249–257
17. Hu Y, Chen YQ, Li L et al (2016) Microstructure and properties of Al/Cu bimetal in liquid–solid compound casting process. Trans Nonferrous Met Soc China 26(6):1555–1563
18. Hajjari E, Divandari M, Razavi SH et al (2011) Dissimilar joining of Al/Mg light metals by compound casting process. J Mater Sci 46(20):6491–6499
19. Schwankl M, Himmler D, Urban M et al (2018) Optimization of mechanical properties of Al-Al-compound castings by adapted heat treatment. Adv Eng Mater 20(12):1800400
20. Schwankl M, Wedler J, Koerner C (2016) Wrought Al-cast Al compound casting based on zincate treatment for aluminum wrought alloy inserts. J Mater Process Technol 238:160–168
21. Jiang WM, Fan ZT, Li C (2015) Improved steel/aluminum bonding in bimetallic castings by a compound casting process. J Mater Process Technol 226:25–31
22. Koerner C, Schwankl M, Himmler D (2014) Aluminum–aluminum compound castings by electroless deposited zinc layers. J Mater Process Technol 214:1094–1101
23. Rubner M, Gunzl M, Koerner C et al (2011) Aluminium–aluminium compound fabrication by high pressure die casting. Mater Sci Eng A 528(22-23):7024–7029
24. Papis KJM, Hallstedt B, Loeffler JF et al (2008) Interface formation in aluminium-aluminium compound casting. Acta Mater 56(13):3036–3043
25. Feng J, Ye B, Zuo LJ et al (2017) Bonding of aluminum alloys in compound casting. Metall Mater Trans A 48(10):4632–4644
26. Ren QS, Zhao CZ, Li ZB et al (2015) Microstructure and mechanical properties of Mg/Al bimetallic composite fabricated by compound casting. Mater Res Innov 19:S73–S78
27. Jiang ZL, Fan ZT, Jiang WM et al (2018) Interfacial microstructures and mechanical properties of Mg/Al bimetal produced by a novel liquid-liquid compound casting process. J Mater Process Technol 261:149–158
28. Li XB, Xiong SM, Guo ZP (2016) Characterization of the grain structures in vacuum-assist high-pressure die casting AM60B alloy. Acta Metall Sin (Engl Lett) 29(7):619–628

29. Li XB, Xiong SM, Guo ZP (2016) Correlation between porosity and fracture mechanism in high pressure die casting of AM60B alloy. J Mater Sci Technol 32(1):54–61
30. Yu WB, Ma CS, Ma YH et al (2021) Correlation of 3D defect-band morphologies and mechanical properties in high pressure die casting magnesium alloy. J Mater Process Technol 288:116853
31. Su CY, Li DJ, Wang J et al (2020) Enhanced ductility in high-pressure die casting Mg-4Ce-xAl-0.5Mn alloys via modifying second phase. Mater Sci Eng A 773:138870
32. Margetis D (2009) Homogenization of reconstructed crystal surfaces: Fick's law of diffusion. Phys Rev E 79(5):052601

Figures

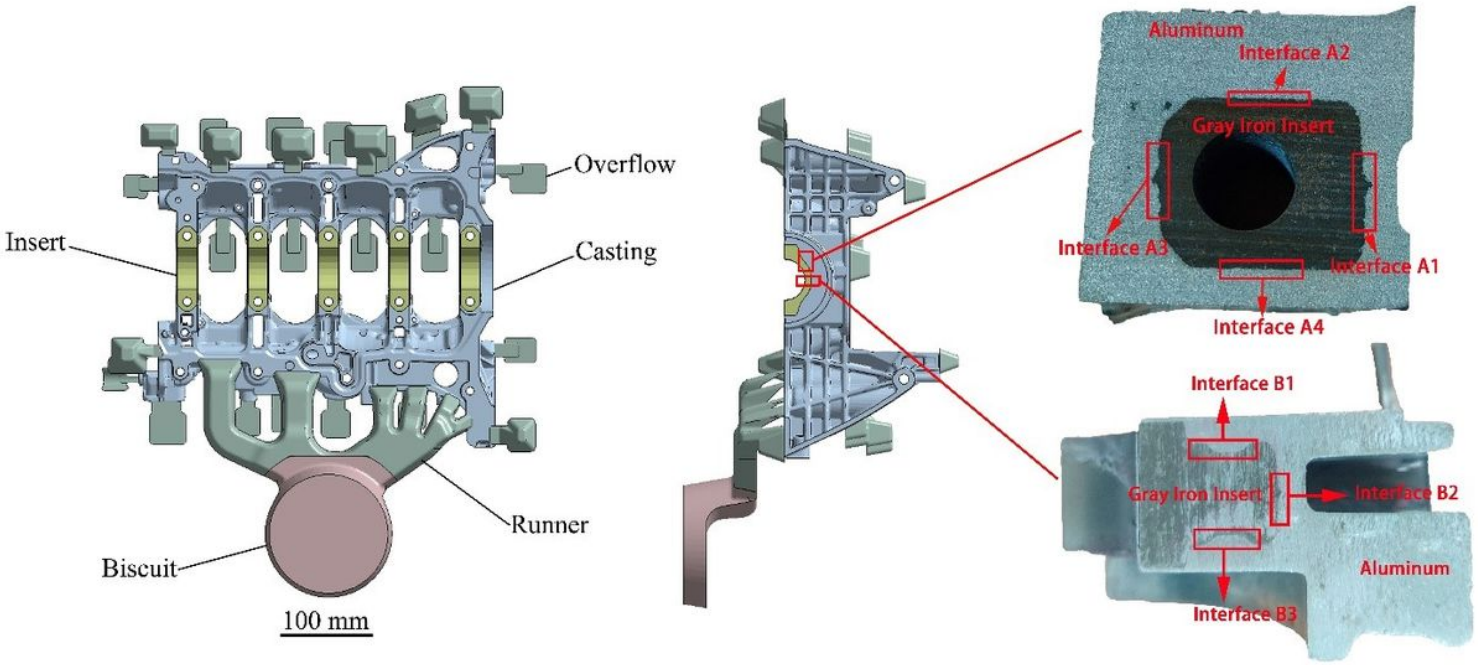

Figure 1

Configuration of the practical bimetallic casting and illustration of the locations of specimens extracted for microstructure characterization

Figure 2

Appearance of the gray iron inserts: (a) no treatment except for being cleaned; (b) salt membrane plating; (c) electrogalvanizing

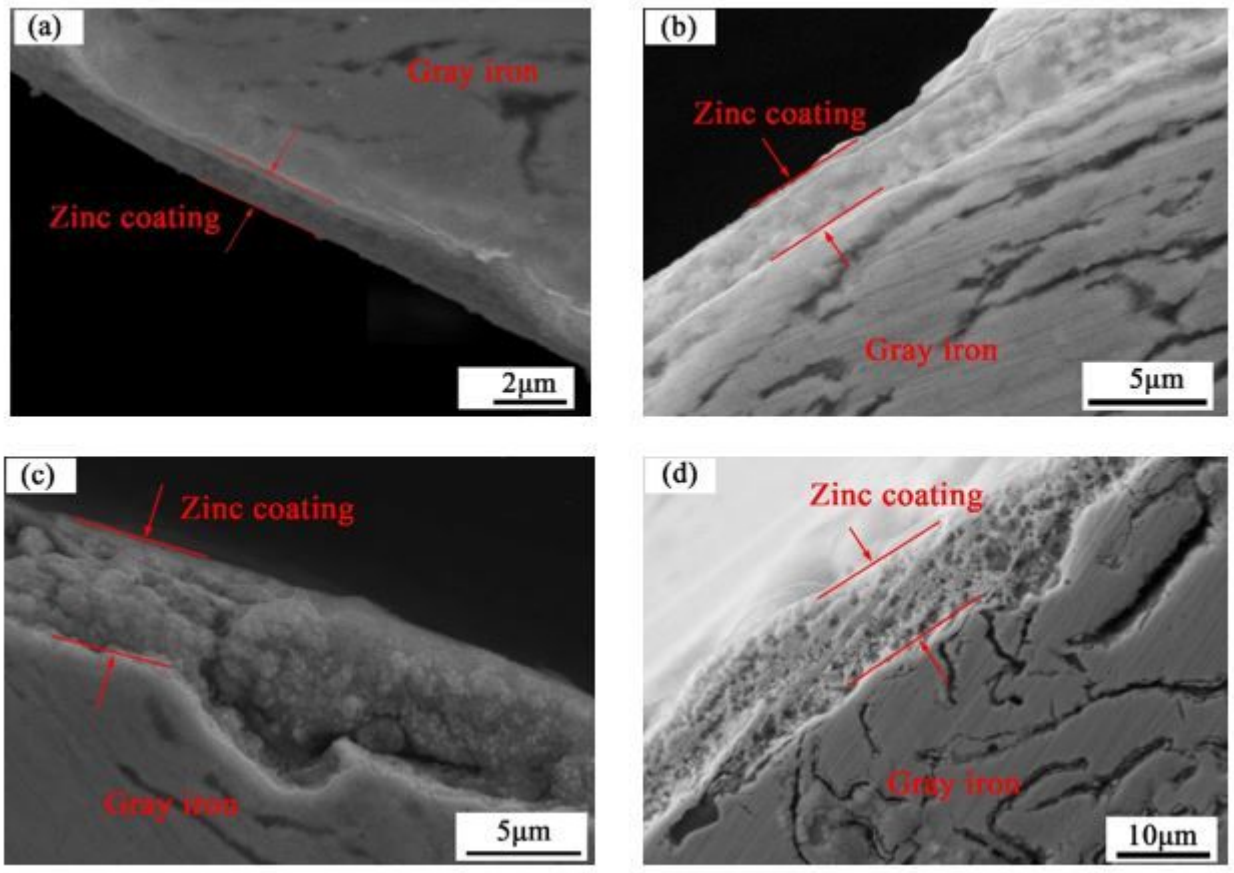

Figure 3

Cross section morphology of the gray iron inserts and thickness of zinc coating: (a) zinc barrel plating for 1 hour; (b) zinc barrel plating for 2 hours; (c) zinc barrel plating for 3 hours; (d) zinc rack plating for 1 hour

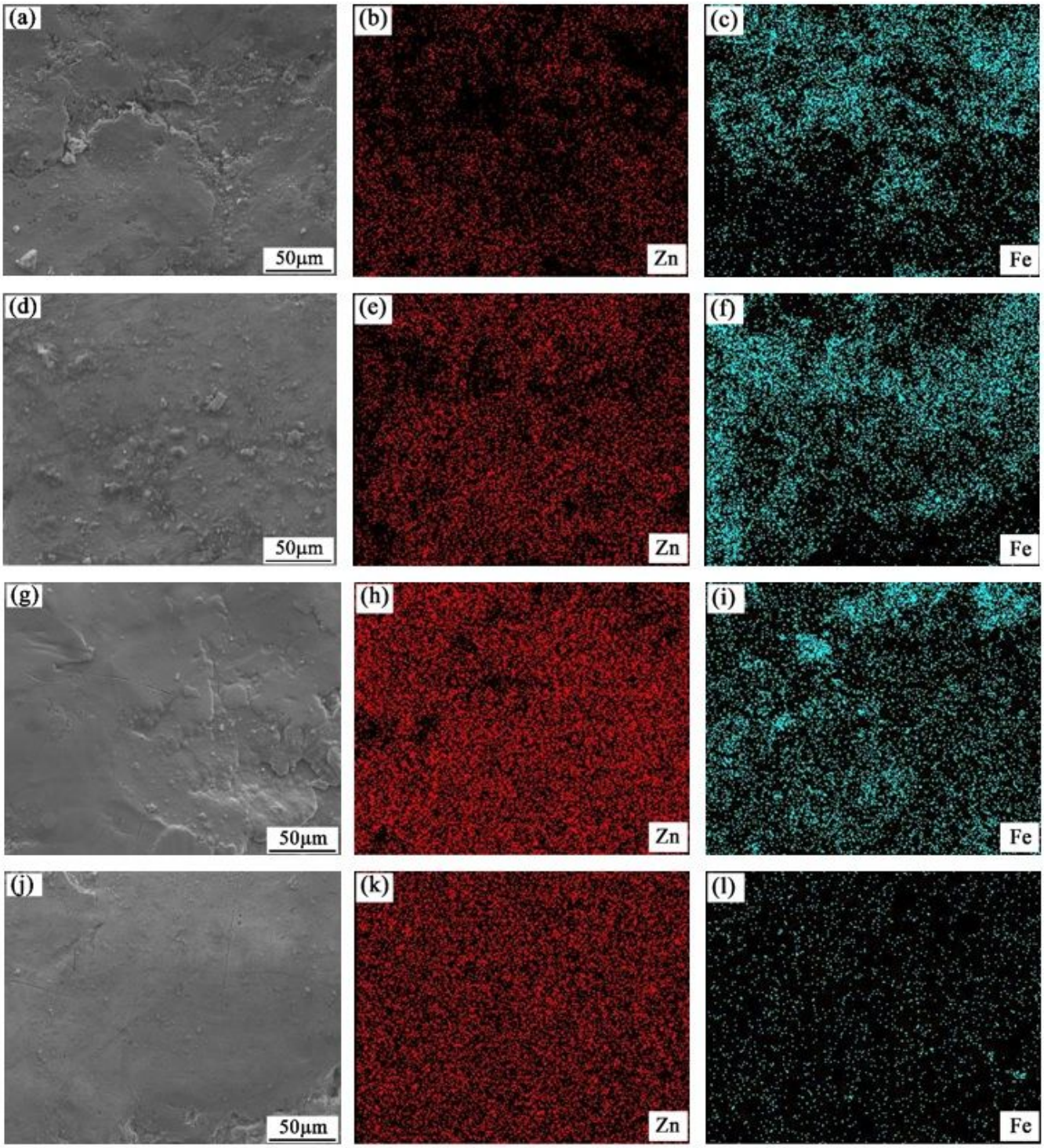

Figure 4

Surface micro-morphology of the gray iron inserts and the corresponding EDS mapping results: (a-c) zinc barrel plating for 1 hour; (d-f) zinc barrel plating for 2 hours; (g-i) zinc barrel plating for 3 hours; (j-l) zinc rack plating for 1 hour

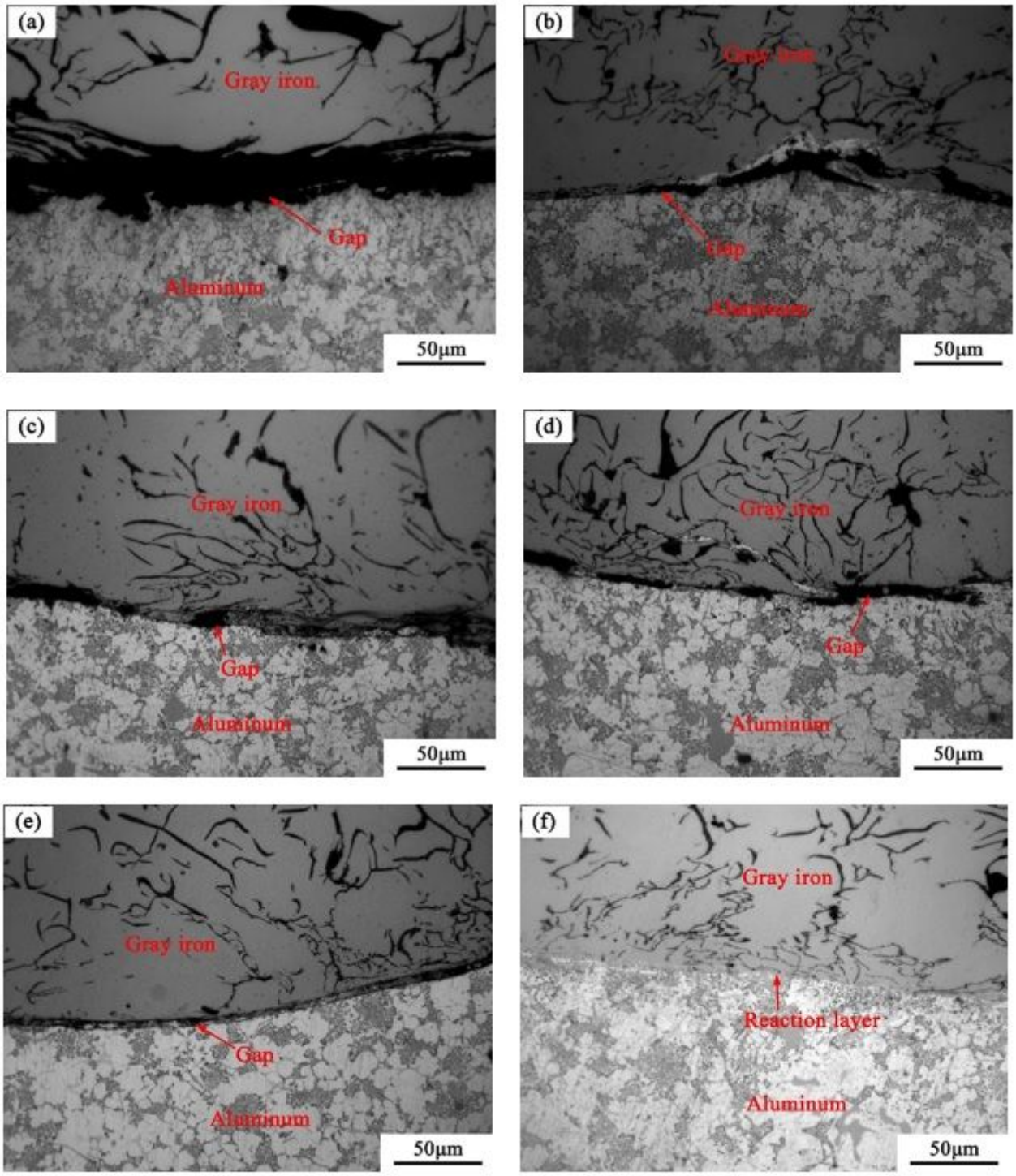

Figure 5

OM images of the microstructure at the bonding interface “A4”of bimetallic castings with different surface treatment methods of the gray iron inserts: (a) no treatment except for being cleaned; (b) salt membrane plating; (c) zinc barrel plating for 1 hour; (d) zinc barrel plating for 2 hours; (e) zinc barrel plating for 3 hours; (f) zinc rack plating for 1 hour

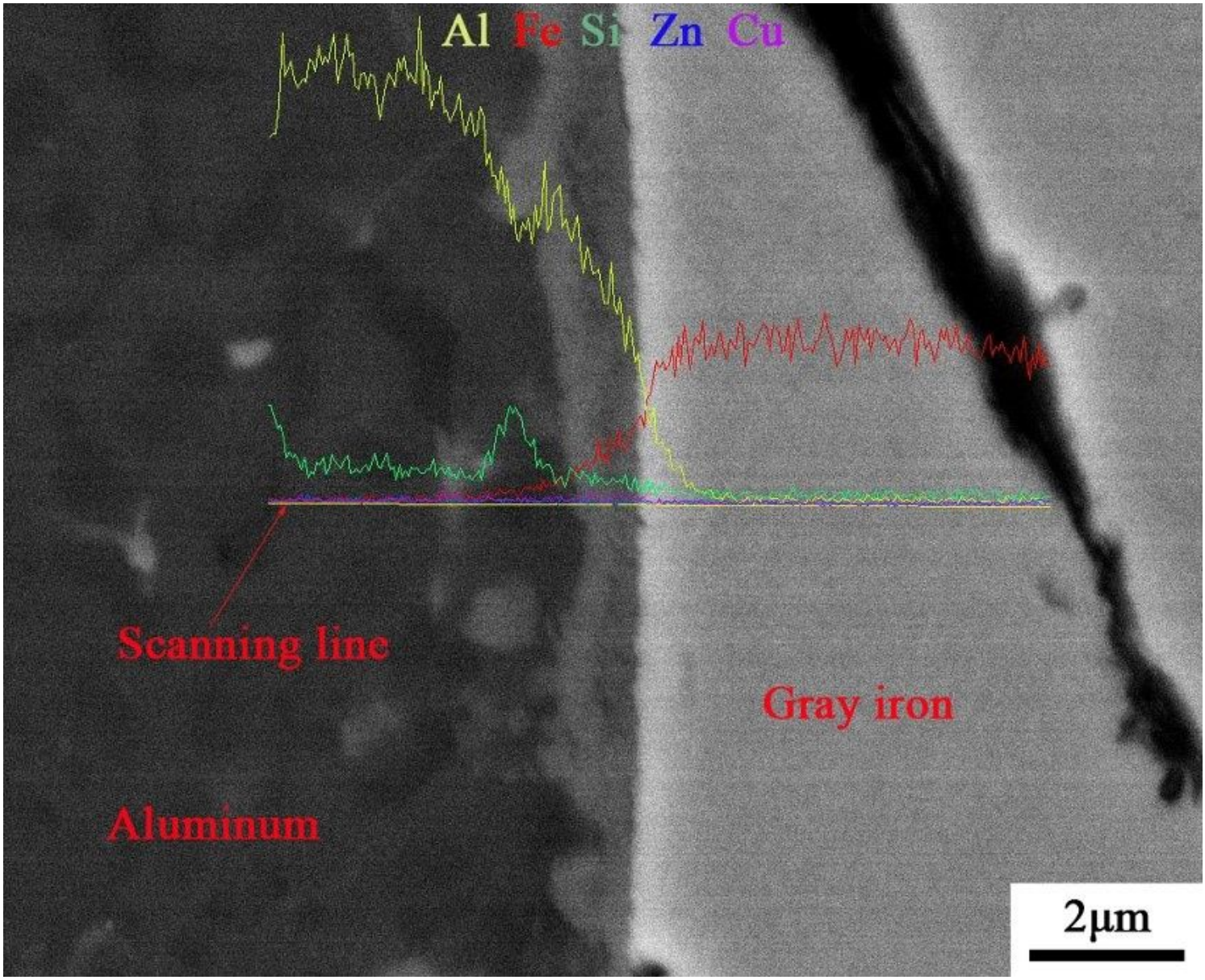

Figure 6

High magnification SEM image of the interfacial microstructure shown in figure 5(f) and the corresponding EDS line scanning results

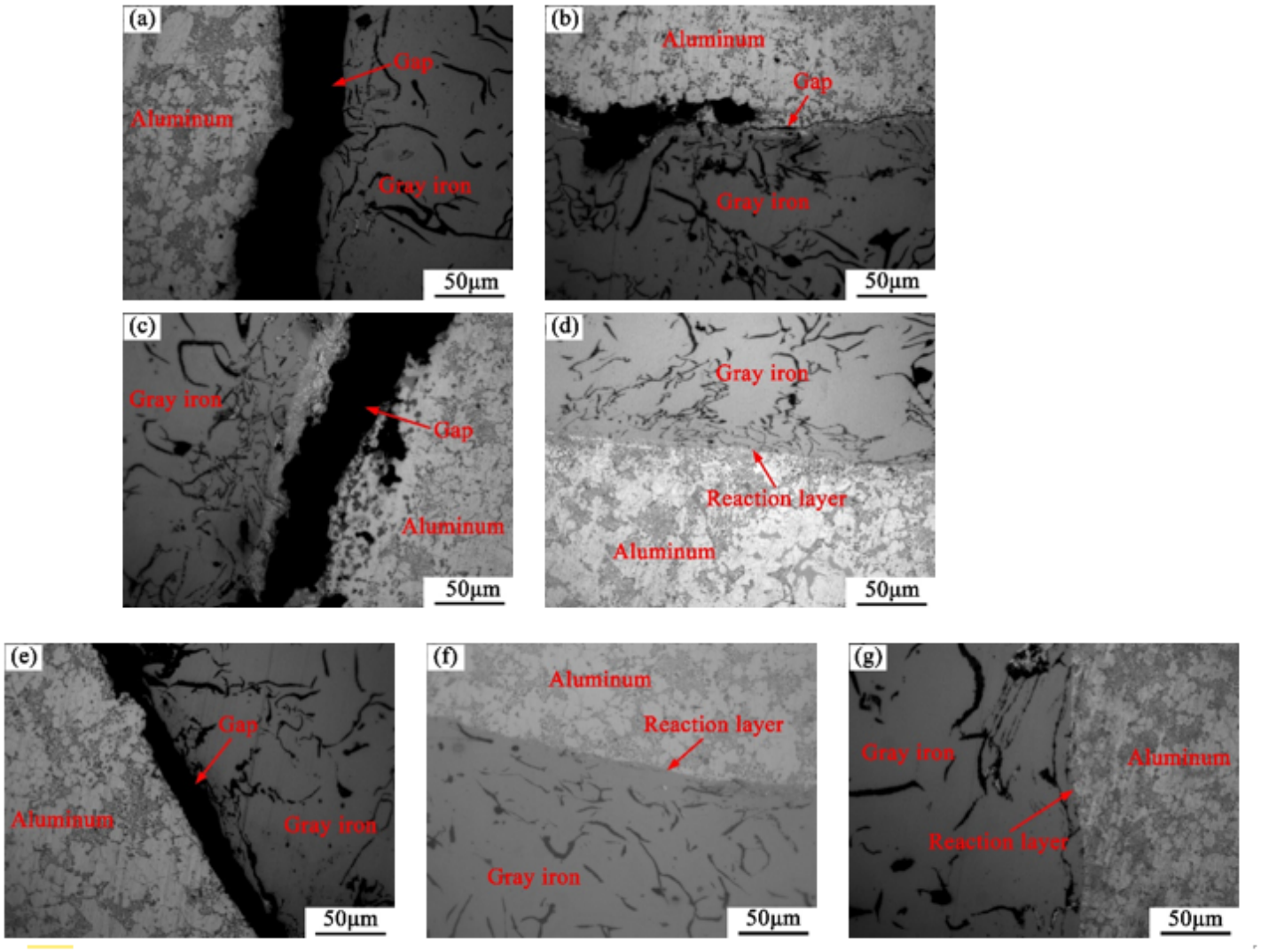

Figure 7

OM images of the microstructure at different bonding interfaces of the bimetallic casting with a treatment of zinc rack plating for 1 hour on surface of the gray iron inserts: (a) A1; (b) A2; (c) A3; (d) A4; (e) B1; (f) B2; (g) B3

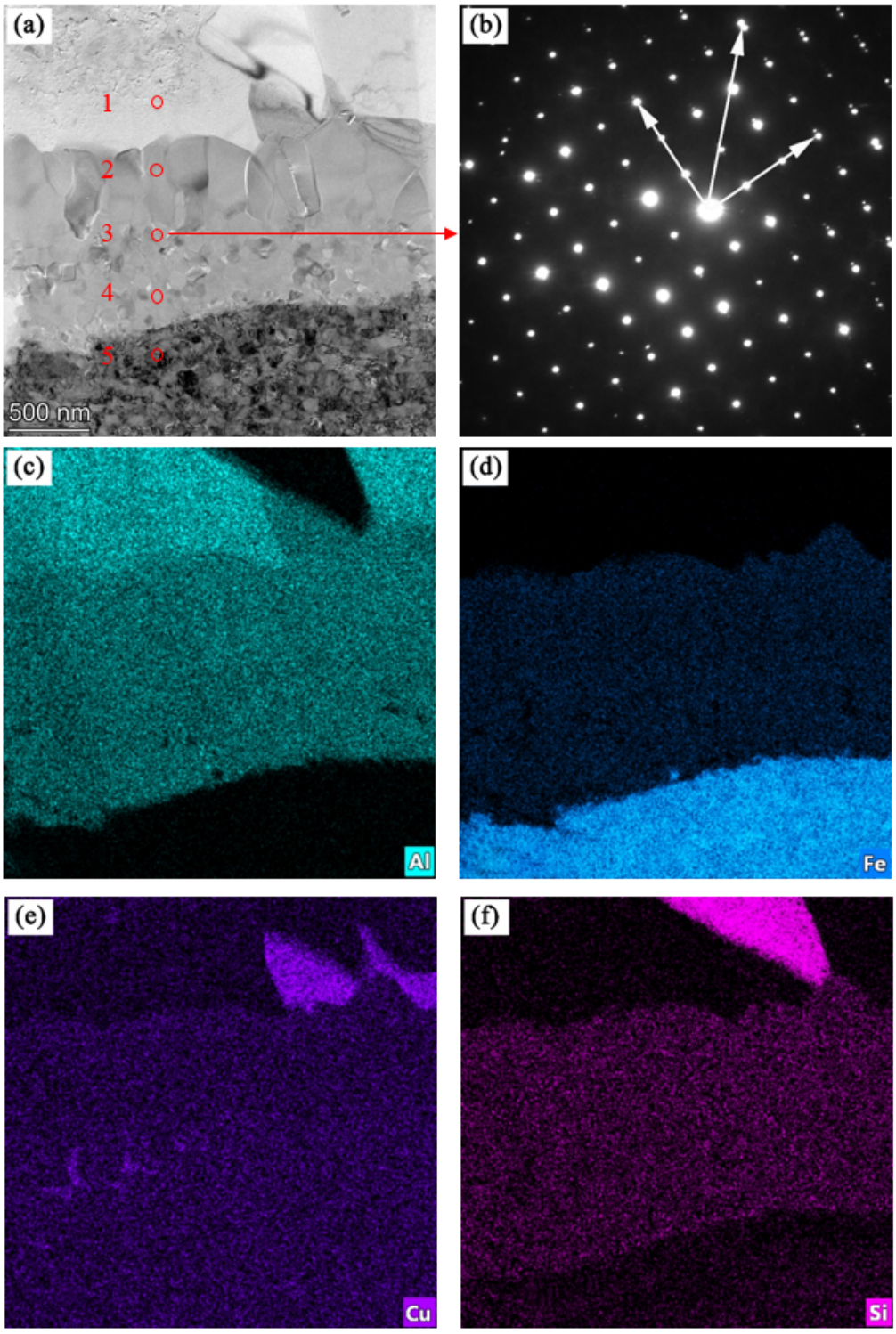

Figure 8

Element distribution and phase identification in the interfacial layer with metallurgical bonding: (a) TEM bright-field image showing interfacial microstructure; (b) microbeam electron diffraction pattern of point 3; (c-f) the corresponding EDS mapping results

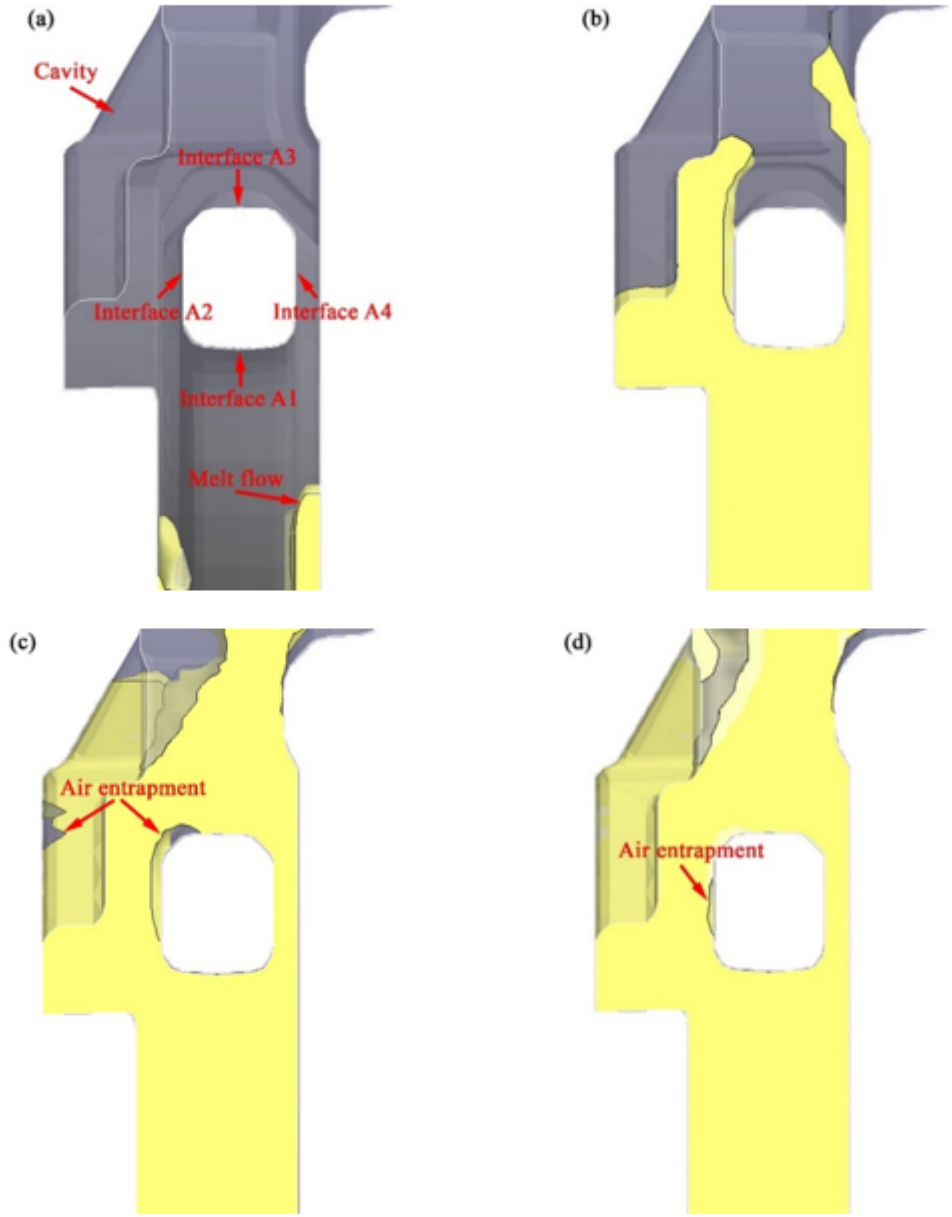

Figure 9

Simulated results of mold filling near section A during the HPDC process at different times: (a) 0.3199 s; (b) 0.3233 s; (c) 0.3287 s; (d) 0.3302 s

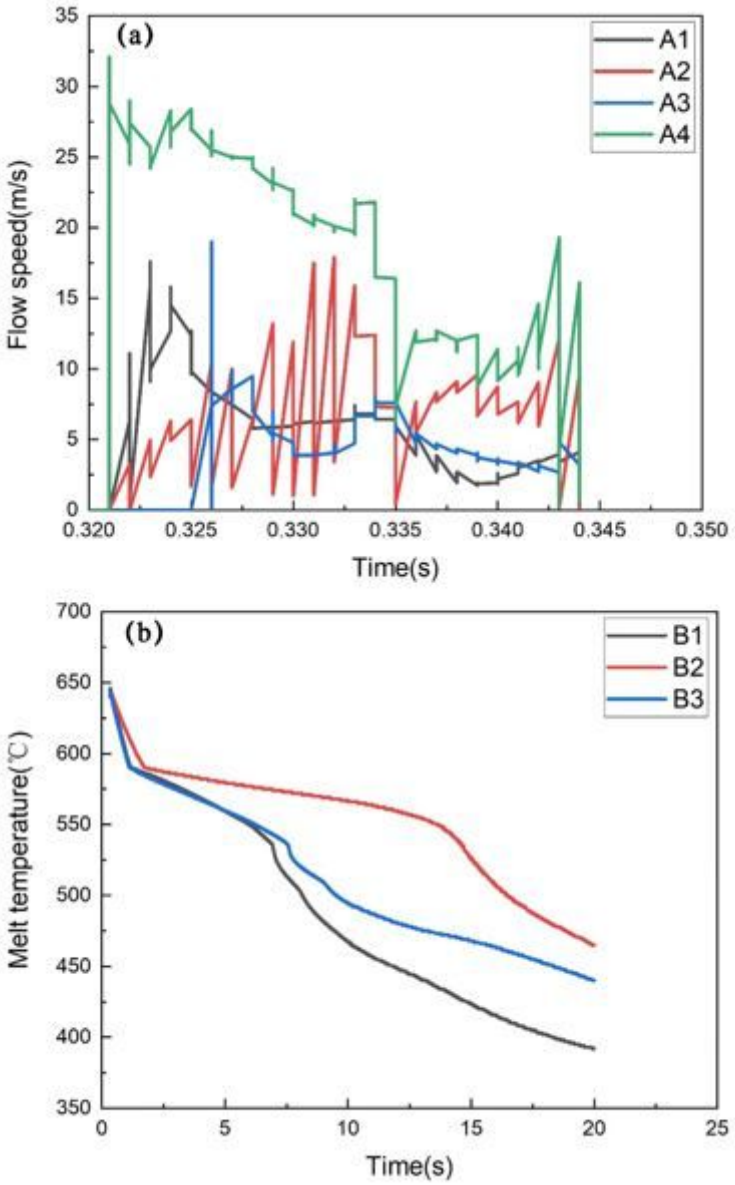

Figure 10

Simulated results of the variation trend of the melt flow speed and temperature at different interfaces: (a) melt flow speeds at interfaces A1-A4; (b) melt temperatures at interfaces B1-B3 (Note: for each interface, the simulated data is exacted from the center point to represent the whole interface.)

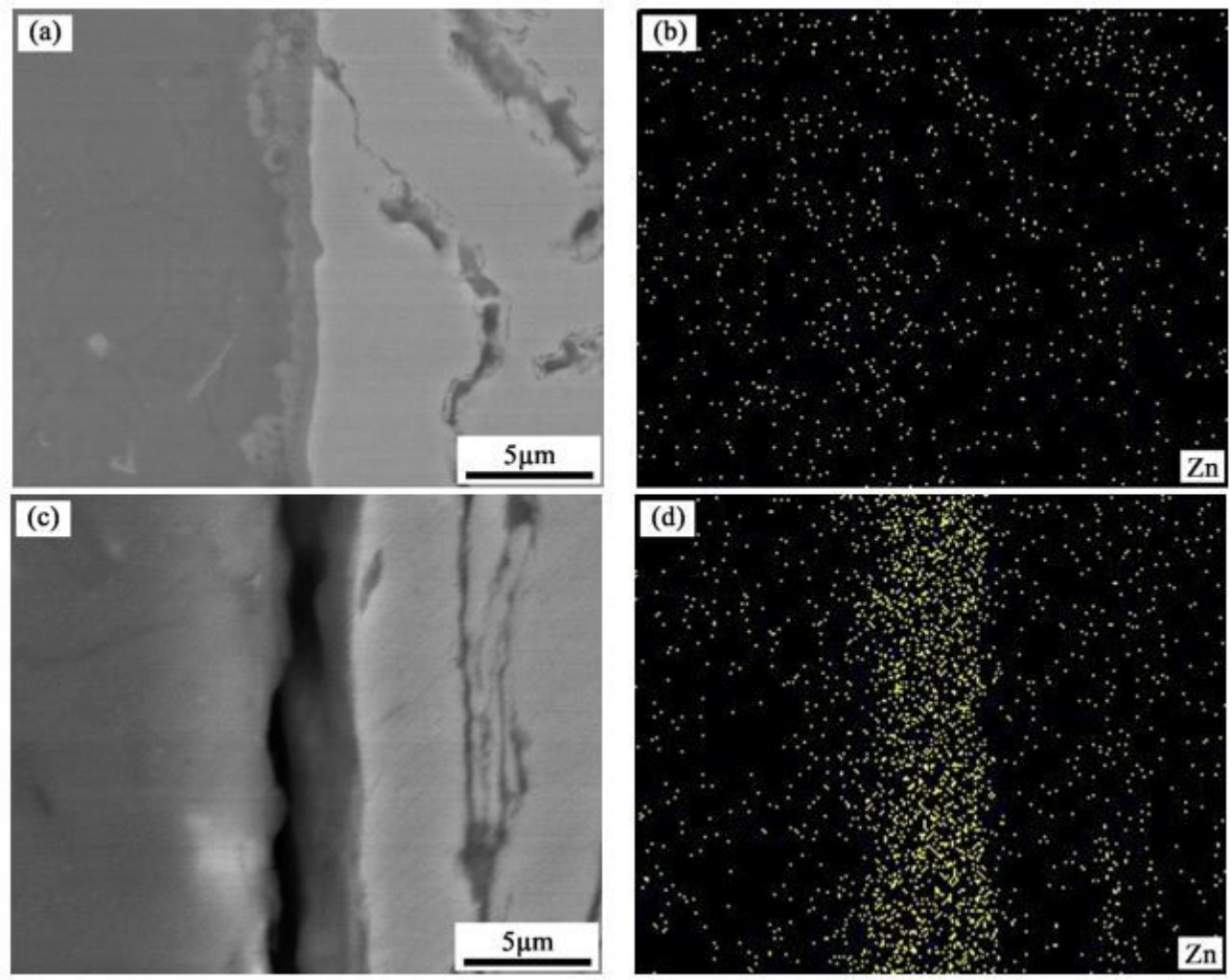

Figure 11

SEM images of the interfacial microstructure and the corresponding EDS mapping results of the zinc element: (a-b) interface with metallurgical bonding; (c-d) interface without metallurgical bonding